ACS OMEGA

Article

Cite This: ACS Omega 2018, 3, 9476−9486

http://pubs.acs.org/journal/acsodf

Imaging pH Dynamics Simultaneously in Two Cellular Compartments Using a Ratiometric pH-Sensitive Mutant of mCherry

Megha Rajendran,[†,‡] Benjamin Claywell,[†] Emily P. Haynes,[†] Umi Scales,[†] Chace K. Henning,[†] and Mathew Tantama*[,†,‡,§]

[†]Department of Chemistry, [‡]Institute for Integrative Neuroscience, and [§]Institute of Inflammation, Immunology, and Infectious Disease, Purdue University, 560 Oval Drive, P.O. Box 68, West Lafayette, Indiana 47907, United States

Supporting Information

ABSTRACT: The regulation of pH is essential for proper organelle function, and organelle-specific changes in pH often reflect the dynamics of physiological signaling and metabolism. For example, mitochondrial energy production depends on the proton gradient maintained between the alkaline mitochondrial matrix and neutral cytosol. However, we still lack a quantitative understanding of how pH dynamics are coupled between compartments and how pH gradients are regulated at organelle boundaries. Genetically encoded pH sensors are well suited to address this problem because they can be targeted to specific subcellular locations and they facilitate live, single-cell analysis. However, most of these pH sensors are derivatives of green and yellow fluorescent proteins that are not spectrally compatible for dual-compartment imaging. Therefore, there is a need for ratiometric red fluorescent protein pH sensors that enable quantitative multicolor imaging of spatially resolved pH dynamics. In this work, we demonstrate that the I158E/Q160A mutant of the red fluorescent protein mCherry is an effective ratiometric pH sensor. It has a pK_a of 7.3 and a greater than 3-fold change in ratio signal. To demonstrate its utility in cells, we measured activity and metabolism-dependent pH dynamics in cultured primary neurons and neuroblastoma cells. Furthermore, we were able to image pH changes simultaneously in the cytosol and mitochondria by using the mCherryEA mutant together with the green fluorescent pH sensor, ratiometric-pHluorin. Our results demonstrate the feasibility of studying interorganelle pH dynamics in live cells over time and the broad applicability of these sensors in studying the role of pH regulation in metabolism and signaling.

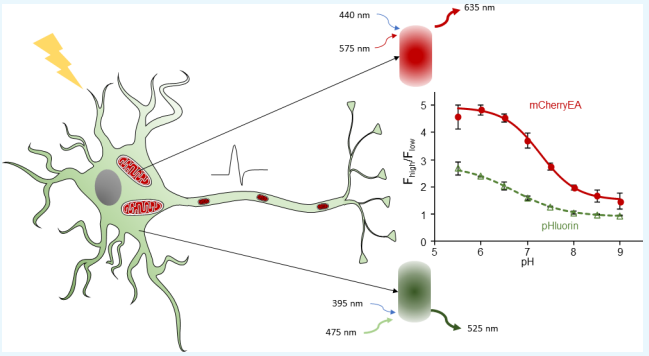

INTRODUCTION

In eukaryotic cells, pH compartmentalization is critical for cellular processes, such as mitochondrial energy production, protein degradation in lysosomes, and post-translational protein modification in the endoplasmic reticulum.[1,2] In the brain, for example, organelle pH gradients are essential for proper neurophysiology. The acidification of synaptic vesicles provides the proton motive force for neurotransmitter loading, and the alkalinization of the mitochondrial matrix provides the proton motive force for adenosine 5′-triphosphate (ATP) synthesis, both of which are required for the energetically expensive process of neurotransmission.[3,4] Because neurotransmission is fundamentally a pH-dependent process, pH is also a useful indicator of activity. For example, transient pH fluctuations in the cytosol of neurons occur due to proton and ion fluxes and mitochondrial pH fluctuates in response to energy consumption during action potential generation.[5−7]

Aberrant changes in pH are also commonly seen in diseases. For example, significant pH changes are seen during neurological disorders such as stroke and ischemia, where pH dynamics during hypoxia plays an important role in cell survival.[1,8] In cancer, altered pH homeostasis can occur[9] and the Warburg effect and metabolic reprogramming can cause intracellular alkalinization and extracellular acidification, both of which may play important roles in cell survival.[10−12] Furthermore, regulation of organelle pH has been linked to oncogenic signaling[13,14] but we still need new pH sensors to accurately study organelle pH changes in the context of the entire cell.

In biological imaging studies, spatially resolved pH dynamics are commonly visualized using pH-sensitive dyes, such as BCECF or SNARF,[15] and genetically encoded green and yellow fluorescent protein-based pH sensors, such as pHluorin and SypHer.[16,17] Genetically encoded sensors are advantageous because they can be targeted to subcellular locations. However, to study the role of proton exchange and buffering between different compartments in pH regulation, we need a toolbox of both green and red fluorescent pH sensors for

Received: April 4, 2018
Accepted: August 6, 2018
Published: August 20, 2018

DOI: 10.1021/acsomega.8b00655
ACS Omega 2018, 3, 9476−9486

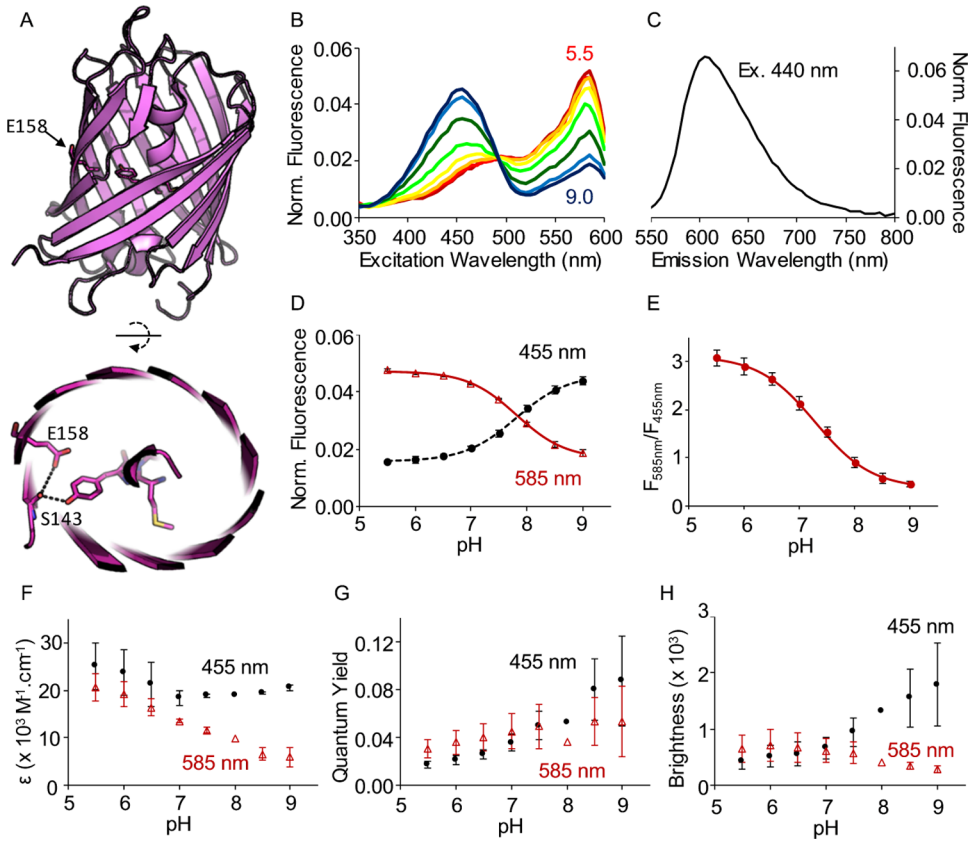

Figure 1. Characterization of purified mCherryEA in solution. (A) Structure of wild-type mCherry (PDB 2H5Q) showing the location of the E158 mutation relative to the chromophore. (B) The pH-dependent fluorescence excitation and (C) emission spectra (λ_{ex} = 440 nm) (n = 6). Fluorescence was normalized to total integrated fluorescence. (D) The pH titration curves for the fluorescence intensity with 455 nm (black, dashed) and 585 nm (red, solid) excitation, with emission at 630 nm. (E) The pH titration curve for the F_{585nm}/F_{455nm} ratio (n = 7). The pH titration curves for the (F) extinction coefficient, (G) quantum yield (QY), and (H) brightness (ε·QY) (n = 2). Data were fit to a Boltzmann equation, ratio = minimum + (maximum − minimum)/(1 + exp((pH − pK_a)/slope)). Errors are standard deviation (std).

multiplex imaging. Currently, many of the red fluorescent protein (RFP) sensors, such as pHTomato,[18] pHuji,[19] and mNectarine,[20] report pH changes on the basis of fluorescence intensity alone. These sensors have high dynamic range and are very useful for the detection of events such as synaptic vesicle release.[21] However, ratiometric sensors are better suited for quantifying pH changes because they are insensitive to variations in sensor concentration and photobleaching, which facilitates the comparison of pH dynamics between independent experiments. The ratiometric red fluorescent protein pH sensor pHRed[22] has been used to monitor pH fluctuations in mitochondria[23] and to measure peroxisomal pH.[24] However, pHRed has a pK_a of 6.9, which limits its sensitivity in alkaline compartments because it exhibits smaller changes in its signal at pH greater than 8. The availability of spectral variants and pH sensors with a range of pK_a values would facilitate the study of pH changes in various cellular compartments.

In this study, we demonstrate that the I158E/Q160A mutant of mCherry, originally reported by Piatkevich et al.,[25] is an effective ratiometric red fluorescent protein pH sensor. We characterize the pH-dependent fluorescence properties of the mCherry mutant protein in solution, and we also characterize its pH sensing performance in live cells. To demonstrate its use in biological studies, we show that it reports pH dynamics caused by changes in neuronal activity and metabolism. Furthermore, we demonstrate that it is spectrally compatible with the green fluorescent pH sensor ratiometric-pHluorin, facilitating the visualization of pH changes in mitochondria and the cytosol simultaneously within the same live cell.

RESULTS

Characterization of mCherryEA as a Ratiometric pH Sensor. We first demonstrated that the mCherry(I158E/Q160A) mutant, which we refer to as "mCherryEA", is a ratiometric pH sensor. The I158E and Q160A mutations were originally engineered to support excited-state proton transfer (ESPT) in mCherry to generate a long Stokes shift (LSS) variant (Figure 1A).[25] This mutant has not been used as a long Stokes shift RFP because at neutral pH, it exhibits two excitation peaks corresponding to the protonated and deprotonated chromophore, with a single emission peak (Figure 1B). However, we hypothesized that existence of the two peaks would instead make the mutant an effective ratiometric pH sensor because it is proposed that the protonation state of Glu158 is sensitive to the pH of the surrounding solution,[25] resulting in pH-dependent protonation of the chromophore.

To determine whether the mCherryEA mutant exhibits a pH-dependent ratiometric change in the excitation spectra peaks, we characterized the pH response of purified mCherryEA protein in solution. The mutant showed pH-dependent changes in its excitation spectra with a ratiometric change in excitation peaks at 455 and 585 nm, without a significant spectral shift in the emission peak at 610 nm (Figure

DOI: 10.1021/acsomega.8b00655
ACS Omega 2018, 3, 9476−9486

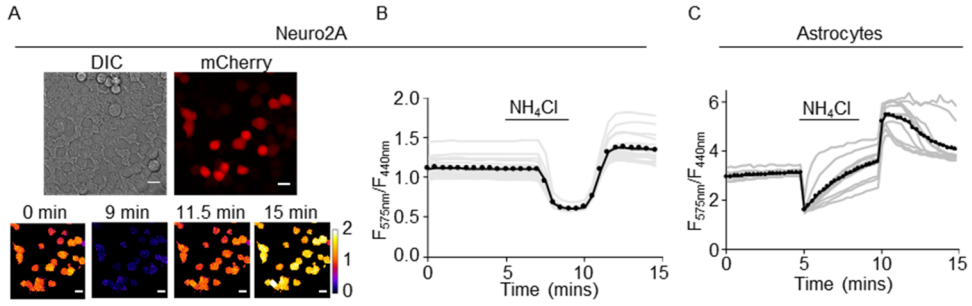

Figure 2. mCherryEA reports live-cell pH changes in different cell types. (A) Top: differential interference contrast (DIC) and fluorescence images showing the expression of mCherryEA in the cytosol of Neuro2A cells. Bottom: representative pseudocolored image sequence showing changes in the pixel-by-pixel fluorescence ratio over time in response to a transient NH_4Cl pulse. (B) The pH response upon exposure to 10 mM NH_4Cl measured as the F_{575nm}/F_{440nm} ratio over time (n = 20). (C) The pH response in primary astrocytes expressing mCherryEA upon exposure to 10 mM NH_4Cl (n = 11).

1B,C). We did not observe residual green emission from immature chromophore, and thus mCherryEA is compatible with blue, cyan, green, and yellow fluorescent proteins that exhibit spectrally distinct emission peaks. As predicted, the proton-transfer network[25] results in an "inverse" pH dependence with an increase from pH 5.5 to 9, causing a 2.80 ± 0.14-fold increase in the 455 nm peak (protonated form) and 2.54 ± 0.20-fold decrease in the 585 nm peak (deprotonated form), with a pK_a of 7.8 (Figure 1D). Fold change was measured by dividing the highest fluorescence ratio by the lowest fluorescence ratio. The intensity ratio (F_{585nm}/F_{455nm}) showed a 6.90 ± 0.83-fold (n = 7, mean ± std) increase with decrease in pH from 9 to 5.5, and the pK_a was 7.29 ± 0.03 for the ratio response (Figure 1E). The pH response was insensitive to variation of salts (NaCl, KCl, $MgCl_2$, and K-gluconate), oxidative stress (H_2O_2 and dithiothreitol (DTT)), and temperature (25−37 °C) (Figure S-1).

To compare the brightness of the mCherryEA mutant relative to wild-type mCherry, we measured the extinction coefficient (ε) and quantum yield (QY) of each protein in solution. At pH 7.5, the mutant (ε = 11 650 M^{-1} cm^{-1}, QY = 0.05) was dimmer compared to wild-type mCherry (ε = 72 000 M^{-1} cm^{-1}, QY = 0.22).[26] Both the excitation peaks showed an increase in QY with increasing pH (Figure 1F). However, the ε_{530nm} decreased with increasing pH and ε_{440nm} remains relatively unchanged (Figure 1G). The brightness (ε·QY) for the 455 nm peak showed a larger change compared to that of the 585 nm peak, and it drives the dynamic range of the ratio (Figure 1H). These results show that the mCherryEA mutant can serve as a ratiometric pH sensor, and therefore it could be an important addition to the toolset of quantitative pH sensors. However, due to the relatively low brightness of the purified protein, we next characterized the sensor expressed in live cells and found it to be well suited for live-cell ratiometric imaging.

Live-Cell Ratiometric pH Imaging. To test mCherryEA as a pH sensor in cellular imaging, we expressed the protein in mammalian cells. The brightness of mCherryEA was comparable to that of pHRed in several mammalian cell lines using exactly the same illumination and imaging conditions (Figures 2 and S-2), and we did not observe any cell toxicity during extended imaging sessions that lasted over 2 h. Differences in sensor characteristics in live cells compared with purified protein measurements have been observed for other fluorescent proteins and sensors, although the exact reasons are unknown.[27,28] Thus, despite the low ε and QY measured for purified protein in solution, in live cells, mCherryEA exhibits sufficient brightness to provide a high fluorescence signal over the background.

We next tested mCherryEA's pH response by exposing the cells to ammonium chloride (NH_4Cl). It is well-established that exposure to NH_4Cl causes a transient alkalinization and reacidification upon washout.[29] The responsiveness of the mutant was demonstrated in Neuro2A cells expressing mCherryEA in the cytosol (Figure 2A). The cells were exposed to 10 mM NH_4Cl for 5 min and then washed with imaging solution. The pH response was determined by measuring the ratio F_{575nm}/F_{440nm} for single cells over time (Figure 2A). As expected, the addition of NH_4Cl caused alkalinization of the cytosol, followed by reacidification upon removal of NH_4Cl (Figure 2B). We found that mCherryEA exhibited a 2.3 ± 0.2-fold change in ratio signal (n = 20, mean ± std) in response to the NH_4Cl transient, which was comparable to the 4.2 ± 0.7-fold change observed for pHRed (n = 29, mean ± std) (Figures 2B and S-2). We saw similar responses in cultured primary astrocytes (Figures 2C and S-3) and in HEK-293 cells (Figure S-3). Note that the lag in pH response to NH_4Cl is caused by the slow perfusion delay and variability in mixing in the live-cell imaging chamber, which also contributes to overall differences in the response. Interestingly, we observed that primary astrocytes regulate cytosolic pH more strongly than Neuro2A cells. That is, the astrocytes exhibited a rebound neutralization during the NH_4Cl exposure, which was not observed in Neuro2A cells (Figure 2B,C). It is not clear if this is an active or passive homeostatic mechanism, but future experiments could address the energy dependence of the response by pairing mCherryEA with one of the currently available green fluorescent ATP sensors.[30−32]

We did observe that long-term expression of both wild-type mCherry and mutant mCherryEA resulted in the formation of red fluorescent puncta in cultured astrocytes after several days (Figure S-3). This may be due to protein accumulation in lysosomes, which has been observed for other red fluorescent proteins.[33−35] To avoid complications caused by puncta formation, all subsequent experiments were carried out 2 days after transfection when neurons and Neuro2A cells did not show any puncta and therefore did not interfere with its use or analysis.

Live-Cell pH Calibration. To calibrate the pH response, we performed an in situ pH titration in Neuro2A cells, expressing cytoplasmic mCherryEA using the ionophore

DOI: 10.1021/acsomega.8b00655
ACS Omega 2018, 3, 9476−9486

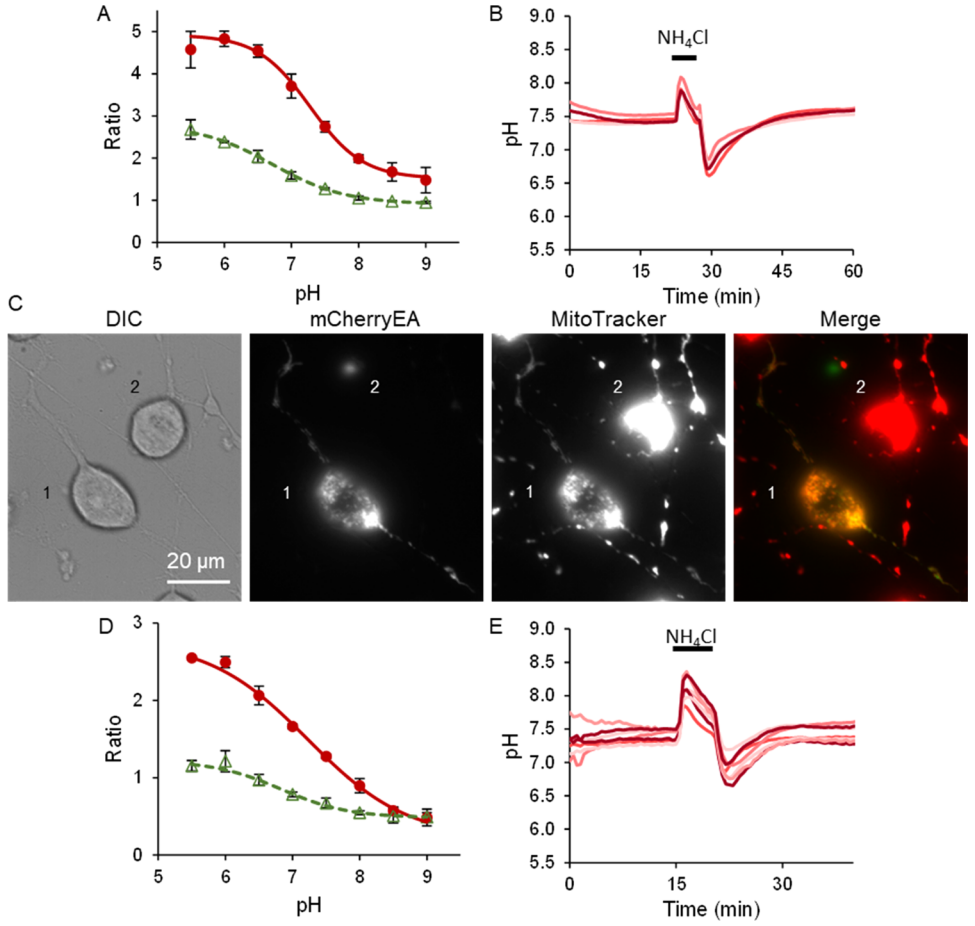

Figure 3. In situ pH calibration of mCherryEA in the cytosol and mitochondria live cells. (A) pH titration of Neuro2A cells expressing cytosolic mCherryEA (red line, n = 6, 10 cells each) or ratiometric-pHluorin (green dashed line, n = 3, 10 cells each) using nigericin. (B) pH change upon exposure to a transient 10 mM NH_4Cl pulse in Neuro2A cells expressing cytosolic mCherryEA that was calibrated using nigericin at the end of the experiment (n = 4). (C) Example DIC and fluorescence images of a Neuro2A cell showing colocalization of mito-mCherryEA and MitoTracker Deep Red. Cell 1 expressed mito-mCherryEA, but cell 2 was not transfected. Cell 1 shows colocalization (yellow) of mito-mCherryEA (green) and MitoTracker (red). (D) pH titration of Neuro2A cells expressing mito-mCherryEA (red line) and mito-ratiometric-pHluorin (green dashed line) using nigericin plus monensin (n = 3, 4–15 cells each). (E) pH change upon exposure to a transient 10 mM NH_4Cl pulse in Neuro2A cells expressing mito-mCherryEA that were calibrated using nigericin plus monensin at the end of the experiment (n = 7). Bars indicate std.

nigericin. Nigericin is a K^+/H^+ ionophore, which equilibrates the intracellular pH and extracellular pH when high-potassium imaging solution is used.[36] The cells were exposed to nigericin solutions to clamp cytosolic pH from pH 5.5 to 9, and steady-state values were measured over a period of 15–30 min (Figure S-4). mCherryEA in cells has a pK_a of 7.31 ± 0.01 (n = 3, mean ± std) (Figure 3A), consistent with the pK_a measured with the purified protein in solution (Figure 1E). We also carried out an end-of-experiment nigericin pH calibration after exposing cells to an ammonium chloride transient pulse, demonstrating that it is possible to normalize ratio signals into pH values (Figures 3B and S-5).

The pK_a of mCherryEA also makes it well suited for studying pH changes in the mitochondria matrix, which can fluctuate between neutral and alkaline conditions (pH 7–8).[17,37] We first demonstrated efficient targeting of mito-mCherryEA in Neuro2A cells using the mitochondrial stain, MitoTracker Deep Red, and high-magnification images confirm colocalization of mito-mCherryEA and MitoTracker (Pearson correlation coefficient 0.93 ± 0.06, n = 12 cells) (Figures 3C and S-6). The in situ pH titration of Neuro2A cells expressing mito-mCherryEA was carried out using nigericin plus monensin to clamp mitochondrial pH from pH 5.5 to 9,[17] and we measured a pK_a of 7.18 ± 0.09 (n = 3, mean ± std) similar to that of both purified protein and in situ cytosolic values (Figure 3D). Again, we carried out an end-of-experiment pH calibration using nigericin plus monensin following an ammonium chloride treatment to demonstrate that ratio signals can be normalized to mitochondrial pH values (Figure 3E). Interestingly, we observed that mitochondrial pH resided near neutral pH, as has been observed for HeLa cells in other studies.[17]

For comparison to mCherryEA, ratiometric-pHluorin[16] is a green fluorescent pH sensor that is also based on a mutated single fluorescent protein. In the cytoplasm, mCherryEA exhibited a maximum fold change of $ratio_{max}/ratio_{min}$ = 3.84 ± 0.91 (mean ± std, n = 6), which is similar to ratiometric-pHluorin expressed in the cytosol of cells ($ratio_{max}/ratio_{min}$ = 2.83 ± 0.20, pK_a = 6.38 ± 0.77, n = 3) (Figure 3A). The maximum fold change was similar for mCherryEA in mitochondria ($ratio_{max}/ratio_{min}$ = 4.42 ± 1.08, mean ± std). However, mito-ratiometric-pHluorin showed a dampened dynamic range ($ratio_{max}/ratio_{min}$ = 1.36 ± 0.16, pK_a = 6.83 ± 0.10, mean ± std, n = 3) (Figure 3D).

DOI: 10.1021/acsomega.8b00655
ACS Omega 2018, 3, 9476–9486

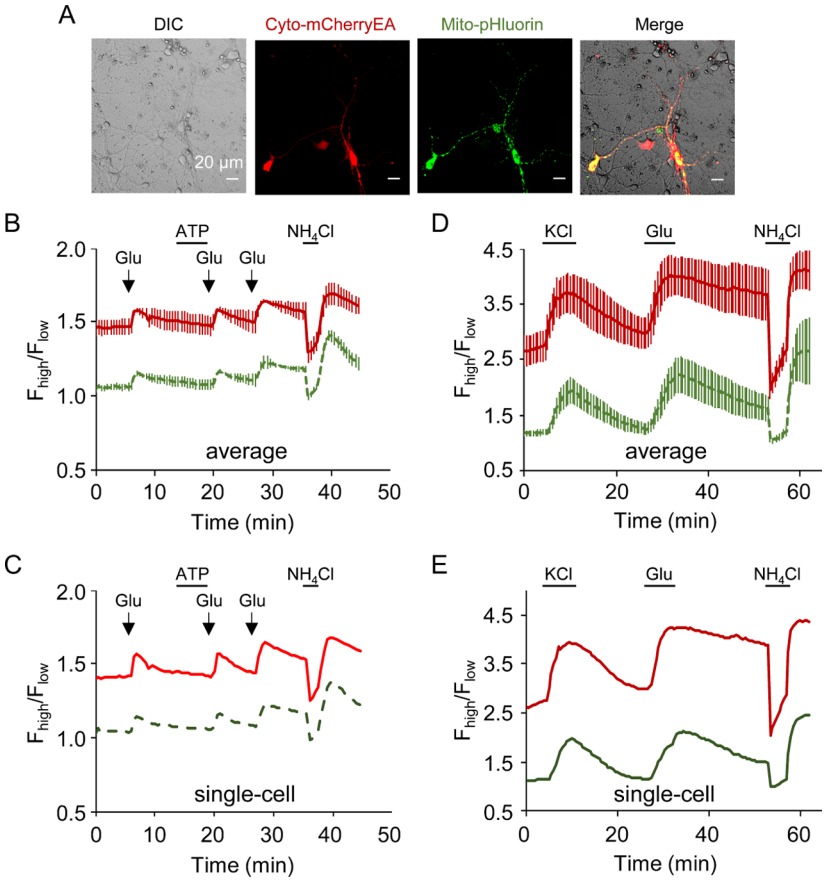

Figure 4. Activity-dependent pH changes in neurons. (A) Representative images showing cortical neurons: DIC, cytosolic mCherryEA (red, λ_{ex} = 575 nm, λ_{em} = 632 nm), mitochondrial ratiometric-pHluorin (green, λ_{ex} = 475 nm; λ_{em} = 525 nm), and merged overlay. (B) Average pH change over time in the cytosol (red) and mitochondria (green, dashed) upon addition of 10 μM glutamate (arrows) in the presence and absence of 100 μM ATP (n = 3). (C) Example of a single-cell response. (D−E) Hippocampal neurons coexpressing cytosolic mCherryEA and mitochondrial ratiometric-pHluorin. (D) Average pH change over time in the cytosol (red) and mitochondria (green, dashed) upon exposure to 15 mM KCl and 10 μM glutamate for 5 min (n = 11). (E) Example of a single-cell response. Cells were treated with 10 mM NH_4Cl at the end of the experiment to validate the sensor response. Bars indicate std.

Thus, we have demonstrated that mCherryEA can be used for calibrated pH measurements in the cytosol and mitochondria of live cells. Ideally, in situ pH calibrations are carried out on a cell-by-cell basis at the end of each experiment to transform the ratio signal into an absolute pH value.[17] However, in practice, ionophores and permeabilization reagents such as nigericin and monensin can cause cell death in sensitive cell types such as primary neurons or after experimental paradigms that already cause significant cell stress and the low yield of successful calibrations can be prohibitive. Despite this complication, relative pH changes within a compartment can be measured more easily and have proven sufficient for studying many physiological processes, including metabolism and neuronal activity.[38−40] Therefore, we next demonstrated that mCherryEA can be used together with ratiometric-pHluorin to measure relative changes in compartment-specific pH, taking advantage of the fact that the spectral cross talk between mCherryEA and ratiometric-pHluorin is minimal (≤3%). Although the ratio signals that we measure cannot be used to directly compare absolute differences in pH between compartments, they can be used to observe correlations between relative pH changes. We conducted two proof-of-concept experiments. First, we demonstrated that both cytosolic and mitochondrial pH exhibit activity-dependent acidification in neurons. To do this, we expressed mCherryEA in cytosol and ratiometric-pHluorin in mitochondria. Second, we demonstrated that relative changes in cytosolic and mitochondrial pH correlate with metabolic inhibition. To do this, we also demonstrate that mCherryEA and ratiometric-pHluorin can be used in either compartment.

Neuronal Activity-Dependent pH Dynamics. Neuronal activity involves membrane depolarization, and membrane depolarization results in the acidification of neurons.[8,41] Membrane depolarization can be caused by neurotransmitters such as glutamate or a rise in external potassium chloride, and both proton fluxes through channels and metabolic generation of acid equivalents can contribute to the pH dynamics.[42,43] To test the utility of mCherryEA in visualizing this activity-dependent acidification, we expressed mCherryEA in the cytosol of cultured mouse hippocampal neurons (Figure 4A). Upon transient stimulation with 10 μM glutamate, we were able to visualize acidification in the cytosol, as expected (Figures 4B,C first arrow and S-7). This was followed by wash-in of 100 μM ATP before a second pulse of glutamate in the presence of ATP (Figure 4B,C second arrow). ATP was then washed out prior to a third glutamate application (Figure 4B,C third arrow). The activity-dependent acidification of the cytosol could be observed with repeated glutamate stimulation, and it was not modified by the application of neuromodulators, such as extracellular ATP acting on neuronal purinergic

DOI: 10.1021/acsomega.8b00655
ACS Omega 2018, 3, 9476−9486

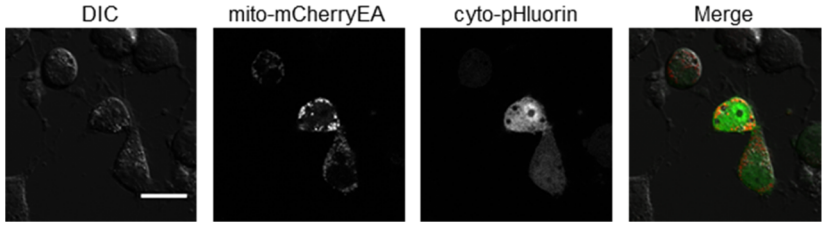

Figure 5. Confocal microscopy. Dual-compartment imaging with mito-mCherryEA and cyto-ratiometric-pHluorin. Scale bar is 20 μm.

receptors.[44] To validate that mCherryEA was responsive to both acidic and alkaline changes in pH, we exposed neurons to a transient pulse of NH_4Cl. Cells exhibited a biphasic response, demonstrating that it is functionally responsive in neurons, similar to other cell types (Figure 2). Because energy metabolism contributes significantly to activity-dependent acidification, we also investigated pH dynamics more closely in both the cytosol and mitochondria.

Neuron excitation is a highly energy consuming process, requiring increased glycolysis and mitochondrial respiration for ATP production. Thus, the increased energy demand drives pH changes in both the cytosol and the mitochondrial matrix, and we used a dual pH sensor imaging approach to test how strongly the compartment-specific pH dynamics is coupled to activity. By coexpressing cytosolic mCherryEA and mitochondria-targeted ratiometric-pHluorin[45] in the same neurons (Figures 4 and S-8), we were able to observe synchronous activity-dependent pH changes with similar dynamics in cytosol and mitochondria. Notably, the spectral cross talk between the mCherryEA red fluorescence and ratiometric-pHluorin green fluorescence channels is minimal ($\lesssim$3%) and does not account for the synchronous changes in cytosolic and mitochondria pH. Thus, the ratio signals report that activity-dependent acidification occurred in each compartment. Although we were unable to carry out pH calibrations due to the toxicity of nigericin and monensin to the cultured neurons, the responsivity of both sensors was validated at the end of the experiment by exposing the cells to NH_4Cl. The activity-dependent pH responses observed in both the cytosol and mitochondria could indicate coupling of neuronal activity to mitochondrial ATP synthesis or uncoupling of pH compartmentation due to increased Ca^{2+} flux. For example, Azarias et al. saw glutamate-induced acidification in mitochondria of astrocytes, which they report was due to loss of cytosol-mitochondrial pH gradient. They also saw pH-dependent loss of metabolism in mitochondria.[46] Further calibration and studies with metabolic sensors would help us better understand the effect of increased neuronal activity on pH and neuron metabolism. Overall, in this proof-of-concept study, we validated that mCherryEA can be used to measure pH dynamics in cultured neurons. We were also able to observe activity-dependent pH changes in different compartments by expressing mCherryEA in the cytosol and ratiometric-pHluorin in the mitochondria of the same cell.

We next tested whether simultaneous imaging of mCherryEA and ratiometric-pHluorin could reveal compartment-specific differences in metabolism-dependent pH dynamics. Since the pK_a of mCherryEA also makes it well suited for studying pH changes in the neutral to alkaline range in mitochondria, we set out to test the utility of mCherryEA in measuring mitochondrial pH dynamics. We confirmed the efficient localization of mCherryEA and ratiometric-pHluorin using confocal imaging to demonstrate that mCherryEA could be efficiently targeted to the mitochondrial matrix when co-transfected with cytosolic ratiometric-pHluorin (Figure 5).

The mCherryEA sensor showed excellent mitochondrial targeting when co-expressed, and therefore we next studied the metabolism-dependent pH changes in a neuroblastoma cell line using well-established inhibitors for glycolytic and oxidative phosphorylation pathways.[47,48]

Metabolism-Dependent pH Dynamics. Metabolism and pH are strongly coupled, with perturbations in the metabolic pathway known to cause pH changes.[1,48] In cancer cells, increased glycolytic activity is known to cause acidification of tumor extracellular environment and alkalinization of the cytosol.[10,12,49] Recent studies have also implicated a link between organelle pH and oncogenic signaling.[50,51] For example, Kondapalli et al. report increased luminal pH due to mutations in Na^+/H^+ exchanger (NHE9) in patient glioblastomas.[13] However, studies on compartment-specific pH changes in neuroblastoma due to metabolic changes are lacking.

To investigate this with our dual sensor imaging strategy, we studied pH changes in the Neuro2A mouse neuroblastoma cell line coexpressing ratiometric-pHluorin and mitochondria-targeted mCherryEA (Figures 6A–C and S-9). Cells were grown in the presence of glucose or in the absence of glucose, using galactose-supplemented media.[52] Cells were then imaged during sequential treatment with metabolic inhibitors to reveal pH changes linked to glycolysis versus mitochondrial respiration. To inhibit glycolysis, the cells were first exposed to iodoacetic acid (IAA). IAA inhibits the glycolytic enzyme glyceraldehyde-3-phosphate dehydrogenase and is frequently used to inhibit glycolysis in a variety of cell types, including Neuro2A cells, as determined by measurement of ATP, reduced nicotinamide adenine dinucleotide, and other metabolic parameters.[30,53−57] To next inhibit mitochondrial electron transport and oxidative phosphorylation, cells were exposed to a combination of the mitochondrial membrane ionophore, carbonyl cyanide-*p*-trifluoromethoxyphenylhydrazone (FCCP), and the ATP synthase inhibitor, oligomycin.[58−60]

As expected, metabolic inhibition with 1 mM IAA caused a small decrease in pH in the cytosol, which is consistent with glycolytic inhibition. Although the pH change before (ratio = 1.39 $\pm$ 0.04, mean $\pm$ std, n = 3) and after (ratio = 1.48 $\pm$ 0.05) IAA addition is not significant for the population average (p = 0.28, n = 3), the pH change is significant ($p < 0.05$) in the cytosol of individual cells, highlighting the power of single-cell analysis to reveal differences obscured by ensemble means. The pH change in the mitochondria before (ratio = 0.90 $\pm$ 0.04) and after (ratio = 0.90 $\pm$ 0.02) IAA addition was not significant (p = 0.80) for the population average (n = 3), but two cells show significant pH decreases ($p \leq 0.015$) (Figure 6B,C). Further calibration would be required to compare the difference in responses between the compartments, but we

DOI: 10.1021/acsomega.8b00655
ACS Omega 2018, 3, 9476−9486

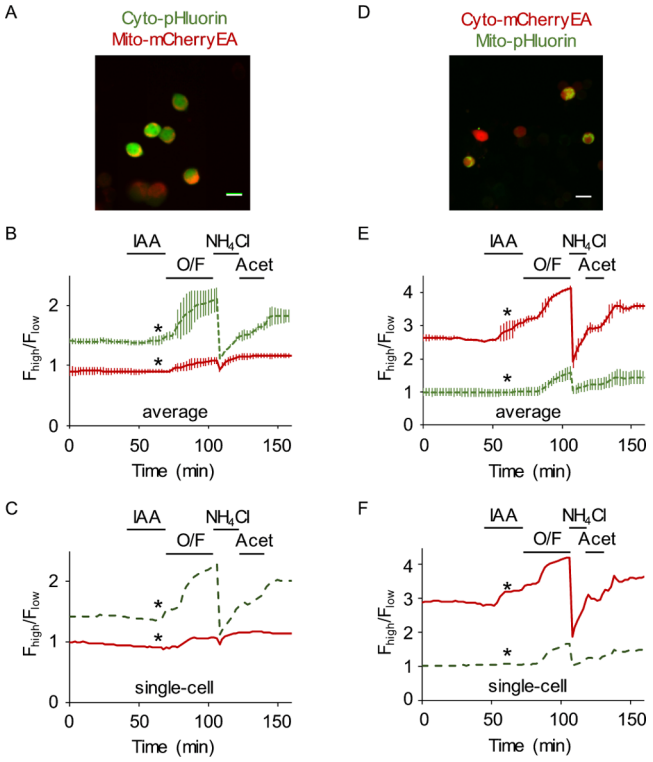

Figure 6. Metabolic inhibition causes differential acidification in the cytosol vs mitochondria. (A) Representative overlay image showing Neuro2A cells expressing cytosolic ratiometric-pHluorin and mitochondria mCherryEA. (B) Average pH change over time in the cytosol (green, dashed) and mitochondria (red). Treatment with the glycolytic inhibitor 1 mM iodoacetic acid (IAA) caused minor acidification in the cytosol with significant difference in the ratio before and after addition of IAA in individual cells. Although, no acidification was detected in mitochondria (asterisks) for the population, two of the three cells showed significant decrease. Treatment with the mitochondrial inhibitors 5 μM oligomycin and 1 μM FCCP (O/F) caused acidification in both compartments, and in particular, the cytosol exhibited large acidification. (D–F) The metabolism-dependent pH dynamics were independent of the sensor. (D) Representative overlay image showing Neuro2A cells expressing cytosolic mCherryEA and mitochondrial ratiometric-pHluorin. (E, F) Similar pH dynamics were observed when the localization of mCherryEA and ratiometric-pHluorin was switched. The sensors were validated at the end of the experiment by adding 30 mM NH_4Cl and 10 mM acetic acid (n = 3, 30 cells total). Error bars are std. Scale bar is 10 μm. mCherryEA (red, λ_{ex} = 575 nm, λ_{em} = 632 nm). ratiometric-pHluorin (green, λ_{ex} = 475 nm, λ_{em} = 525 nm).

were clearly able to observe relative pH changes in each compartment. Subsequent treatment with 1 μM FCCP and 5 μM oligomycin (O/F) blocked oxidative phosphorylation and caused further acidification in the cytosol (before O/F ratio = 1.48 ± 0.05; after O/F ratio = 2.08 ± 0.17, p = 0.06, n = 3) and also in mitochondria (before O/F ratio = 0.90 ± 0.02; after O/F ratio = 1.07 ± 0.05, p = 0.02, n = 3). Individual cells showed a significant decrease in pH in both the compartments (p < 0.001). Although blocking the ATP synthase with oligomycin alone would increase mitochondrial pH, the presence of FCCP causes coupling between mitochondrial and cytosolic pH resulting in acidification of the mitochondria. Interestingly, the metabolism-dependent pH dynamics may be dependent on glycogen stores, fatty acid supply, or gluconeogenic amino acid supply because IAA also caused acidification when glucose is replaced with galactose.[52] The IAA-dependent acidification during galactose replacement indicates that extracellular glucose supply is not strictly required for the effect (Figure S-9). However, future metabolic studies will be needed to explore this further.

Importantly, the compartment-specific differences in pH dynamics are consistent with the compartmentation of metabolic processes and we validated that our observations are not an artifact of the sensors themselves. To do this, we switched the localization of the two sensors, now expressing mCherryEA in the cytosol and ratiometric-pHluorin in the mitochondria. We again observed that FCCP and oligomycin treatment caused the greatest change in pH of the cytosol and of the mitochondria compared with IAA treatment, confirming that the compartment-specific pH dynamics are independent of the specific sensor (Figure 6D–F). We cannot interpret the difference between cytosol and mitochondria dynamics because of the dampened dynamic range in mitochondria, but in the future, additional pH calibration of the sensor in mitochondria and other organelles will enable compartment-specific differences in pH dynamics to be quantified with respect to the physiological process under study.

These studies show the mCherryEA sensor can be used simultaneously with ratiometric-pHluorin to monitor coupled pH changes in two compartments. In addition, the mCherryEA mutant, a ratiometric red pH sensor with a pK_a of 7.3, is well suited for quantitative imaging in neutral to alkaline organelles, such as cytosol (pH 7.2), endoplasmic reticulum (pH 7.2), mitochondria (pH 8), and peroxisome (pH 7).[61]

DISCUSSION AND CONCLUSIONS

We demonstrated here that mCherryEA is a ratiometric red fluorescent pH sensor that adds to the current toolbox of genetically encoded indicators available for multicolor live-cell imaging. An excitation ratiometric sensor exhibits two peaks in its fluorescence excitation spectrum, and for fluorescent protein-based sensors, the peaks are characteristic of the ionization states of the chromophore. The I158E/Q160A mutant of mCherry was originally engineered by Piatkevich et al. to shift the ionization state of the chromophore from the deprotonated to protonated form to generate a long Stokes shift (LSS) mutant.[25] Structural analysis indicated that an aspartate or glutamate at residue 160 could facilitate excited-state proton transfer (ESPT), and therefore the I160E mutation was made to create a proton-relay network between S158, E160, and the hydroxyl group of the chromophore.[25] ESPT mutants have been similarly engineered for LSS mutants of mCherry and other RFPs.[25,62] Piatkevich et al. also showed that the E160 interacts with solvent protons,[25] and we showed here that this interaction makes it a suitable solvent pH sensor. In a similar manner, pHluorin was engineered using the S202H mutation in wild-type green fluorescent protein (GFP). Although wild-type GFP exhibits excitation peaks characteristic of the protonated and deprotonated states, it does not exhibit a ratiometric shift in ionization in response to pH changes. Like the engineered glutamate in mCherryEA, the residue S202, which is involved in the proton-relay network, was mutated to histidine (pK_a = 6.0) in pHluorin to increase its sensitivity to solvent pH. Thus, our work characterizing mCherryEA highlights the utility of engineering ESPT mutants of RFPs to generate new pH sensors.

Interestingly, in our characterization of mCherryEA, we found that despite the low quantum yield and extinction

DOI: 10.1021/acsomega.8b00655
ACS Omega 2018, 3, 9476–9486

coefficient measured from the purified protein, the brightness of mCherryEA expressed in live cells was comparable to that of pHRed under same imaging conditions. Similar photophysical and photochemical differences between solution studies versus live-cell studies have been observed for other fluorescent protein biosensors, but the exact causes are not well understood.[27,28] We then compared the pH sensing characteristics of mCherryEA to that of two other single fluorescent protein-based pH sensors. We found that mCherryEA has a more alkaline pK_a of 7.3 compared to that of both ratiometric-pHluorin and pHRed, making mCherryEA useful for monitoring pH changes in neutral to alkaline compartments. We also found that the dynamic range for mCherryEA (4-fold change) is comparable to that for ratiometric-pHluorin and several commonly used fluorescence resonance energy transfer (FRET) sensors, such as AKAR, EKAR, and JNKAR, which show 1.2−2-fold change in cells.[63−65] In the future, further mutagenesis could help improve the dynamic range of mCherryEA to be comparable to that of the multidomain green fluorescent pH sensor SypHer (10-fold change)[17,27] (Figure S-2) and other FRET-based sensors such as the calcium sensor Twitch (4−10-fold change).[66]

A major contribution of mCherryEA is to enable multicolor live-cell imaging because it is red fluorescent and should be compatible with green fluorescent sensors. As a proof-of-concept, we simultaneously imaged mCherryEA and ratiometric-pHluorin in different compartments in live neurons and neuroblastoma cells. We demonstrated that the negligible spectral cross talk between mCherryEA and ratiometric-pHluorin makes it possible to measure pH changes in the cytosol and mitochondria of the same cell. We observed relative changes in compartment-specific pH that correlated with neuronal activity and metabolic inhibition. However, because the sensors show decreased dynamic range in mitochondria, we could not directly compare the differences in pH between compartments. To compare pH changes between organelles, it is necessary to carry out an in situ pH calibration at the end of each experiment on a cell-by-cell basis, as demonstrated by Poburko et al. for example.[17] We demonstrate that in situ calibrations can be done with cytosolic or mitochondrial-targeted mCherryEA using nigericin and monensin. However, we also found that nigericin and monensin can cause extensive cell death after long metabolic manipulations or with primary neuron cultures, precluding our ability to carry out in situ calibrations in some scenarios. In the absence of calibrated measurements, mCherryEA can still be used to observe relative changes in pH within a compartment.

In conclusion, we demonstrated that the mCherryEA mutant is a red fluorescent, ratiometric pH sensor with pK_a of 7.3, which is more alkaline than other red fluorescent pH sensors such as pHRed. It can be used to measure compartment-specific pH changes simultaneously with green fluorescent pH sensors such as ratiometric-pHluorin in several different cell types, and in principle, it is spectrally compatible with sensors of other analytes that utilize blue, cyan, green, or yellow fluorescent proteins.

METHODS

Materials. Unless otherwise stated, chemicals were purchased from Sigma-Aldrich; molecular biology enzymes were purchased from New England Biolabs (NEB); and cell culture media and supplements were purchased from Invitrogen. Neuro2A and HEK-293 were purchased from ATCC, C57BL/6, and FVB mice were purchased from Charles River Laboratories. MitoTracker Deep Red FM was a kind gift from Dr. Qing Deng at Purdue University.

Molecular Biology. pRSETb-mCherry(wt) and GW1-mCherry(wt) were mutated using the NEB Q5 site-directed mutagenesis kit to generate the mCherry(I158E/Q160A) mutant. Mitochondria-targeted mCherryEA was cloned by fusing a tandem 4xCoxVIII signal sequence[67] to the N-terminus. GW1-ratiometric-pHluorin and GW1-SypHer were generated by subcloning ratiometric-pHluorin from VV064: 1xCox8-ratiometric-pHluorin and SypHer from SypHer-mt into GW1 vector using NEB HiFi reactions. VV064: 1xCox8-ratiometric-pHluorin in the FCK vector was a gift from Adam Cohen (Addgene plasmid # 58502), and SypHer-mt was a gift from Nicolas Demaurex (Addgene plasmid # 48251).

Protein Expression and Purification. pRSETb-mCherryEA was transformed into BL21(DE3) cells and grown in 500 mL of autoinduction media (ForMedium) at 37 °C overnight and transferred to 4 °C for 3 days. Protein was purified using HisTrap Nickel columns (GE Healthcare) according to manufacturer instructions. Purified protein was dialyzed into storage solution (5 mM 3-(*N*-morpholino)propanesulfonic acid (MOPS), 150 mM NaCl, and 5% glycerol, pH 7.4) and stored at −80 °C.

Steady-State Fluorescence Spectroscopy. pH titration was performed in solutions containing 10 mM each of Bis-Tris, MOPS, and Tris plus 100 mM NaCl adjusted to pH values ranging from 5.5 to 9. Protein samples were diluted to 1−2 μM, and fluorescence was measured in a microplate reader (BioTek Synergy H5). The excitation spectrum was measured using a monochromator set to scan from 350 to 600 nm, with emission set at 630 nm. The fluorescence was normalized by calculating the ratio of excitation peaks at 585 by 450 nm. To test for environmental interference, the mutants were titrated in buffered solutions containing either 100 mM NaCl, KCl, or K-gluconate and the addition of 1 mM $MgCl_2$, 1 mM $CaCl_2$, 1 mM H_2O_2, and 3 mM DTT. For temperature dependence, the fluorescence measurement was taken with the reader set to 23, 25, 31, and 37 °C.

Cell Culture and Transfections. Neuro2A (ATCC CCL-131) and HEK-293 (ATCC CRL-1573) cells were cultured at 37 °C in a 5% CO_2 humidified air incubator in Dulbecco's modified Eagle's medium (DMEM) media containing 10% cosmic calf serum (HyClone). Cells were transfected using Effectene (Qiagen) as per manufacturer's instructions and imaged after 2 days.

Neuron and Astrocyte Cultures. All animal procedures were performed in strict accordance with recommendations provided in the National Institutes of Health Guide for the Care and Use of Laboratory Animals, according to protocols approved by the Purdue Animal Care and Use Committee and the Purdue University Laboratory Animal Program to minimize pain and suffering. Cortical and hippocampal neurons were isolated from P0 mice and maintained in Neurobasal media supplemented with 5−25 mM glucose, 0.2 mM pyruvate, 0.5 mM GlutaMAX, B-27, penicillin, and streptomycin (Pen/Strep). Neurons were transfected after 7−9 days using calcium phosphate method.[68] Cortical astrocytes were isolated from P0 to P4 mice and maintained in DMEM/F12 media supplemented with 10% fetal bovine serum and Pen/Strep. Astrocytes were transfected using Lipofectamine 3000 (Invitrogen), as per manufacturer's instructions.

DOI: 10.1021/acsomega.8b00655
ACS Omega 2018, 3, 9476−9486

Extinction Coefficient (ε) and Quantum Yield (QY). The concentration of protein containing mature chromophore was quantified by measuring the absorbance of the protein in 1 M NaOH at 450 nm (ε: 44 000 M^{-1} cm^{-1}), as previously described.[18] Twenty-eight percent of purified mCherryEA corresponded to mature chromophore. The concentration from alkaline denaturation method was used for ε and QY measurements. For ε measurement, absorbance and fluorescence spectra of the protein at dilutions of 5−20 μM were measured. The ε was calculated according to the Beer−Lambert equation. For QY measurement, slopes from absorbance versus fluorescence at different pH were measured with wild-type mCherry as the standard for excitation at 530 nm (QY = 0.22). QY at 440 nm was calculated relative to 530 nm QY.

Sensor Characterization in Live Cells. NH_4Cl: pH response of the sensors in live cells was tested by adding 10 mM NH_4Cl to the imaging solution (mM: 15 *N*-(2-hydroxyethyl)piperazine-*N*′-ethanesulfonic acid (HEPES), 1.25 NaH_2PO_4, 10 glucose, 120 NaCl, 3 KCl, 2 $CaCl_2$, 1 $MgCl_2$, and 3 $NaHCO_3$, pH 7.3). Cytosol pH calibration: Neuro2A cells transfected with mCherryEA or ratiometric-pHluorin were seeded in a multiwell plate and exposed to different pH ranging from 5.5 to 9 in a high-potassium solution (mM: 15 HEPES, 1.25 KH_2PO_4, 10 glucose, 123 KCl, 2 $CaCl_2$, 1 $MgCl_2$, pH 7.3) in the presence of 2−5 μM nigericin.[22,27,60] Mitochondria pH calibration: Neuro2A cells transfected with mito-mCherryEA or mito-pHluorin seeded in a multiwell plate were exposed to pH 5.5−9 in a high-potassium solution (mM: 15 HEPES, 10 glucose, 123 KCl, 20 NaCl, 2 $CaCl_2$, 1 $MgCl_2$) in the presence of 5 μg/mL nigericin and 5 μM monensin. For individual cell calibration, Neuro2A cells were treated with 10 mM NH4Cl. After washing the cells with imaging solution, a three-point calibration was performed with high-potassium solutions buffered at pH 6.0, 7.5, and 8.0.

Live-Cell Imaging. Cells were imaged using an Olympus IX83 fluorescence microscope with a 20×/0.75 NA and 60×/1.35 oil objective illuminated by a Lumencor SpectraX light engine and equipped with an Andor Zyla 4.2 sCMOS camera. Lumencor power levels were typically set at 5−10% for each ratio channel for cytosolic sensor and 15−30% for mitochondrial sensor. mCherryEA and pHRed were excited using 575/25 and 438/29 nm band-pass filters, and emission was collected through a 632/60 nm band-pass filter. Ratiometric-pHluorin was excited using 475/34 and 395/25 nm band-pass filters, and emission was collected through a 525/50 nm band-pass filter. SypHer was excited using 475/34 and 438/29 nm band-pass filters, and emission was collected through a 525/50 nm band-pass filter. The exposure time was set between 50 and 200 ms for all experiments, and fluorescence signals were at least 3-fold above the background in all fluorescence channels. For mCherryEA and pHRed comparison, cells expressing each sensor were imaged on the same days under the exact same illumination and imaging conditions (exposure times, light-emitting diode power, etc.). Neurons were perfused at 1 mL/min with artificial cerebrospinal fluid (mM: 15 HEPES, 120 NaCl, 3 KCl, 2 $CaCl_2$, 1 $MgCl_2$, 3 $NaHCO_3$, 1.25 NaH_2PO_4, 5 glucose, 0.2 pyruvate, and 0.5 glutamax, pH 7.4). To confirm targeting of GW1-4xCox8-mCherryEA, 10 nM MitoTracker Deep Red (Invitrogen) was added to Neuro2A cells expressing mito-mCherryEA and treated as per manufacturer's instruction. High-magnification images were captured using the 60×/1.35 oil objective. MitoTracker Deep Red was excited using 631/28 nm band-pass filter and emission was collected through a ET706/95 nm band-pass filter.

Data Analysis. Images were acquired with IQ (Andor) and analyzed with ImageJ. The mean and background intensities were measured for the images. The ratio was calculated by dividing the background-subtracted means of images excited at the higher wavelength by the lower wavelength. For pixel-by-pixel measurement, fluorescence images were background-subtracted and a threshold was set to reject background pixels. Ratio images were obtained by dividing the images captured by exciting at the higher and the lower excitation wavelengths.

■ ASSOCIATED CONTENT

Supporting Information

The Supporting Information is available free of charge on the ACS Publications website at DOI: 10.1021/acsomega.8b00655.

Additional spectroscopic characterization of protein in solution, sensor characterization with live-cell imaging, calibration details, mitochondrial localization images, and single-cell responses (PDF)

■ AUTHOR INFORMATION

Corresponding Author

*E-mail: mtantama@purdue.edu. Phone: 765-494-5312.

ORCID

Megha Rajendran: 0000-0001-8078-4738

Mathew Tantama: 0000-0002-4072-7680

Notes

The authors declare no competing financial interest.

■ ACKNOWLEDGMENTS

This work was supported by National Institutes of Health Grants R21 NS092010 and R21 EY026425 to M.T., Ralph and Grace Showalter Trust Young Investigator Award to M.T., Purdue Research Foundation support for E.P.H., and Louis Stokes Alliance for Minority Participation support for C.K.H. We thank Saranya Radhakrishnan and Stevie Norcross for assistance with cell culture.

■ REFERENCES

(1) Casey, J. R.; Grinstein, S.; Orlowski, J. Sensors and Regulators of Intracellular pH. *Nat. Rev. Mol. Cell Biol.* **2010**, *11*, 50−61.

(2) Wu, M. M.; Grabe, M.; Adams, S.; Tsien, R. Y.; Moore, H. P. H.; Machen, T. E. Mechanisms of pH Regulation in the Regulated Secretory Pathway. *J. Biol. Chem.* **2001**, *276*, 33027−33035.

(3) Sinning, A.; Hübner, C. A. Minireview: pH and Synaptic Transmission. *FEBS Lett.* **2013**, *587*, 1923−1928.

(4) Nicholls, D. G.; Budd, S. L. Mitochondria and Neuronal Survival. *Physiol. Rev.* **2000**, *80*, 315−360.

(5) Chesler, M.; Kaila, K. Modulation of pH by Neuronal Activity. *Trends Neurosci.* **1992**, *15*, 396−402.

(6) Rossano, A. J.; Chouhan, A. K.; Macleod, G. T. Genetically Encoded pH-Indicators Reveal Activity-Dependent Cytosolic Acidification of Drosophila Motor Nerve Termini in Vivo. *J. Physiol.* **2013**, *591*, 1691−1706.

(7) Kann, O.; Kovács, R. Mitochondria and Neuronal Activity. *Am. J. Physiol.-Cell Physiol.* **2007**, *292*, C641−C657.

(8) Deitmer, J. W.; Rose, C. R. pH Regulation and Proton Signalling by Glial Cells. *Prog. Neurobiol.* **1996**, *48*, 73−103.

(9) Webb, B. A.; Chimenti, M.; Jacobson, M. P.; Barber, D. L. Dysregulated pH: A Perfect Storm for Cancer Progression. *Nat. Rev. Cancer* **2011**, *11*, 671−677.

DOI: 10.1021/acsomega.8b00655
ACS Omega 2018, 3, 9476−9486

(10) Helmlinger, G.; Sckell, A.; Dellian, M.; Forbes, N. S.; Jain, R. K. Acid Production in Glycolysis-Impaired Tumors Provides New Insights into Tumor Metabolism. *Clin. Cancer Res.* **2002**, *8*, 1284−1291.
(11) Estrella, V.; Chen, T.; Lloyd, M.; Wojtkowiak, J.; Cornnell, H. H.; Ibrahim-Hashim, A.; Bailey, K.; Balagurunathan, Y.; Rothberg, J. M.; Sloane, B. F.; Johnson, J.; Gatenby, R. A.; Gillies, R. J. Acidity Generated by the Tumor Microenvironment Drives Local Invasion. *Cancer Res.* **2013**, *73*, 1524−1535.
(12) Schornack, P. A.; Gillies, R. J. Contributions of Cell Metabolism and H+ Diffusion to the Acidic pH of Tumors. *Neoplasia* **2003**, *5*, 135−145.
(13) Kondapalli, K. C.; Llongueras, J. P.; Capilla-González, V.; Prasad, H.; Hack, A.; Smith, C.; Guerrero-Cázares, H.; Quiñones-Hinojosa, A.; Rao, R. A Leak Pathway for Luminal Protons in Endosomes Drives Oncogenic Signalling in Glioblastoma. *Nat. Commun.* **2015**, *6*, No. 6289.
(14) Di Domenico, F.; Foppoli, C.; Blarzino, C.; Perluigi, M.; Paolini, F.; Morici, S.; Coccia, R.; Cini, C.; De Marco, F. Expression of Human Papilloma Virus Type 16 E5 Protein in Amelanotic Melanoma Cells Regulates Endo-Cellular pH and Restores Tyrosinase Activity. *J. Exp. Clin. Cancer Res.* **2009**, *28*, 4.
(15) Han, J.; Burgess, K. Fluorescent Indicators for Intracellular pH. *Chem. Rev.* **2010**, *110*, 2709−2728.
(16) Miesenböck, G.; De Angelis, D. A.; Rothman, J. E. Visualizing Secretion and Synaptic Transmission with pH-Sensitive Green Fluorescent Proteins. *Nature* **1998**, *394*, 192−195.
(17) Poburko, D.; Santo-Domingo, J.; Demaurex, N. Dynamic Regulation of the Mitochondrial Proton Gradient during Cytosolic Calcium Elevations. *J. Biol. Chem.* **2011**, *286*, 11672−11684.
(18) Li, Y.; Tsien, R. W. pHTomato, a Red, Genetically Encoded Indicator That Enables Multiplex Interrogation of Synaptic Activity. *Nat. Neurosci.* **2012**, *15*, 1047−1053.
(19) Shen, Y.; Rosendale, M.; Campbell, R. E.; Perrais, D. pHuji, a pH-Sensitive Red Fluorescent Protein for Imaging of Exo- and Endocytosis. *J. Cell Biol.* **2014**, *207*, 419−432.
(20) Johnson, D. E.; Ai, H. W.; Wong, P.; Young, J. D.; Campbell, R. E.; Casey, J. R. Red Fluorescent Protein pH Biosensor to Detect Concentrative Nucleoside Transport. *J. Biol. Chem.* **2009**, *284*, 20499−20511.
(21) Li, Y.; Tsien, R. W. pHTomato, a Red, Genetically Encoded Indicator That Enables Multiplex Interrogation of Synaptic Activity. *Nat. Neurosci.* **2012**, *15*, 1047−1053.
(22) Tantama, M.; Hung, Y. P.; Yellen, G. Imaging Intracellular pH in Live Cells with a Genetically Encoded Red Fluorescent Protein Sensor. *J. Am. Chem. Soc.* **2011**, *133*, 10034−10037.
(23) Rosselin, M.; Santo-Domingo, J.; Bermont, F.; Giacomello, M.; Demaurex, N. L-OPA1 Regulates Mitoflash Biogenesis Independently from Membrane Fusion. *EMBO Rep.* **2017**, *18*, 451−463.
(24) Godinho, L. F.; Schrader, M. Determination of Peroxisomal pH in Living Mammalian Cells Using pHRed. In *Peroxisomes: Methods and Protocols, Methods in Molecular Biology*; Schrader, M., Ed.; Springer: New York, 2017; pp 181−189.
(25) Piatkevich, K. D.; Malashkevich, V. N.; Almo, S. C.; Verkhusha, V. V. Engineering ESPT Pathways Based on Structural Analysis of LSSmKate Red Fluorescent Proteins with Large Stokes Shift. *J. Am. Chem. Soc.* **2010**, *132*, 10762−10770.
(26) Shaner, N. C.; Campbell, R. E.; Steinbach, P. A.; Giepmans, B. N. G.; Palmer, A. E.; Tsien, R. Y. Improved Monomeric Red, Orange and Yellow Fluorescent Proteins Derived from Discosoma Sp. Red Fluorescent Protein. *Nat. Biotechnol.* **2004**, *22*, 1567−1572.
(27) Matlashov, M. E.; Bogdanova, Y. A.; Ermakova, G. V.; Mishina, N. M.; Ermakova, Y. G.; Nikitin, E. S.; Balaban, P. M.; Okabe, S.; Lukyanov, S.; Enikolopov, G.; Zaraisky, A. G.; Belousov, V. V. Fluorescent Ratiometric pH Indicator SypHer2: Applications in Neuroscience and Regenerative Biology. *Biochim. Biophys. Acta, Gen. Subj.* **2015**, *1850*, 2318−2328.
(28) Balleza, E.; Kim, J. M.; Cluzel, P. Systematic Characterization of Maturation Time of Fluorescent Proteins in Living Cells. *Nat. Methods* **2018**, *15*, 47−51.
(29) Musa-Aziz, R.; Jiang, L.; Chen, L. M.; Behar, K. L.; Boron, W. F. Concentration-Dependent Effects on Intracellular and Surface pH of Exposing Xenopus Oocytes to Solutions Containing NH_3/NH_4^+. *J. Membr. Biol.* **2009**, *228*, 15−31.
(30) Tantama, M.; Martinez-Francois, J. R.; Mongeon, R.; Yellen, G. Imaging Energy Status in Live Cells with a Fluorescent Biosensor of the Intracellular ATP-to-ADP Ratio. *Nat. Commun.* **2013**, *4*, No. 2550.
(31) Yaginuma, H.; Kawai, S.; Tabata, K. V.; Tomiyama, K.; Kakizuka, A.; Komatsuzaki, T.; Noji, H.; Imamura, H. Diversity in ATP Concentrations in a Single Bacterial Cell Population Revealed by Quantitative Single-Cell Imaging. *Sci. Rep.* **2015**, *4*, No. 6522.
(32) Imamura, H.; Nhat, K. P. H.; Togawa, H.; Saito, K.; Iino, R.; Kato-Yamada, Y.; Nagai, T.; Noji, H. Visualization of ATP Levels inside Single Living Cells with Fluorescence Resonance Energy Transfer-Based Genetically Encoded Indicators. *Proc. Natl. Acad. Sci. U.S.A.* **2009**, *106*, 15651−15656.
(33) Costantini, L. M.; Fossati, M.; Francolini, M.; Snapp, E. L. Assessing the Tendency of Fluorescent Proteins to Oligomerize Under Physiologic Conditions. *Traffic* **2012**, *13*, 643−649.
(34) Katayama, H.; Yamamoto, A.; Mizushima, N.; Yoshimori, T.; Miyawaki, A. GFP-like Proteins Stably Accumulate in Lysosomes. *Cell Struct. Funct.* **2008**, *33*, 1−12.
(35) Shemiakina, I. I.; Ermakova, G. V.; Cranfill, P. J.; Baird, M. A.; Evans, R. A.; Souslova, E. A.; Staroverov, D. B.; Gorokhovatsky, A. Y.; Putintseva, E. V.; Gorodnicheva, T. V.; Chepurnykh, T. V.; Strukova, L.; Lukyanov, S.; Zaraisky, A. G.; Davidson, M. W.; Chudakov, D. M.; Shcherbo, D. A Monomeric Red Fluorescent Protein with Low Cytotoxicity. *Nat. Commun.* **2012**, *3*, No. 1204.
(36) Thomas, J. A.; Buchsbaum, R. N.; Zimniak, A.; Racker, E. Intracellular pH Measurements in Ehrlich Ascites Tumor Cells Utilizing Spectroscopic Probes Generated in Situ. *Biochemistry* **1979**, *18*, 2210−2218.
(37) Benčina, M. Illumination of the Spatial Order of Intracellular pH by Genetically Encoded pH-Sensitive Sensors. *Sensors* **2013**, *13*, 16736−16758.
(38) Breckwoldt, M. O.; Armoundas, A. A.; Aon, M. A.; Bendszus, M.; O'Rourke, B.; Schwarzländer, M.; Dick, T. P.; Kurz, F. T. Mitochondrial Redox and pH Signaling Occurs in Axonal and Synaptic Organelle Clusters. *Sci. Rep.* **2016**, *6*, No. 23251.
(39) Lazarenko, R. M.; DelBove, C. E.; Strothman, C. E.; Zhang, Q. Ammonium Chloride Alters Neuronal Excitability and Synaptic Vesicle Release. *Sci. Rep.* **2017**, *7*, No. 5061.
(40) Rathje, M.; Fang, H.; Bachman, J. L.; Anggono, V.; Gether, U.; Huganir, R. L.; Madsen, K. L. AMPA Receptor pHluorin-GluA2 Reports NMDA Receptor-Induced Intracellular Acidification in Hippocampal Neurons. *Proc. Natl. Acad. Sci. U.S.A.* **2013**, *110*, 14426−14431.
(41) Magnotta, V. A.; Heo, H.-Y.; Dlouhy, B. J.; Dahdaleh, N. S.; Follmer, R. L.; Thedens, D. R.; Welsh, M. J.; Wemmie, J. A. Detecting Activity-Evoked pH Changes in Human Brain. *Proc. Natl. Acad. Sci. U.S.A.* **2012**, *109*, 8270−8273.
(42) Esquivel, G.; Schruers, K.; Maddock, R.; Colasanti, A.; Griez, E. Acids in the Brain: A Factor in Panic? *J. Psychopharmacol.* **2010**, *24*, 639−647.
(43) Chesler, M. Regulation and Modulation of pH in the Brain. *Physiol. Rev.* **2003**, 1183−1221.
(44) Khakh, B. S.; North, R. A. Neuromodulation by Extracellular ATP and P2X Receptors in the CNS. *Neuron* **2012**, *76*, 51−69.
(45) Venkatachalam, V.; Cohen, A. E. Imaging GFP-Based Reporters in Neurons with Multiwavelength Optogenetic Control. *Biophys. J.* **2014**, *107*, 1554−1563.
(46) Azarias, G.; Perreten, H.; Lengacher, S.; Poburko, D.; Demaurex, N.; Magistretti, P. J.; Chatton, J.-Y. Glutamate Transport Decreases Mitochondrial pH and Modulates Oxidative Metabolism in Astrocytes. *J. Neurosci.* **2011**, *31*, 3550−3559.

DOI: 10.1021/acsomega.8b00655
ACS Omega 2018, 3, 9476−9486

(47) Perry, S. W.; Norman, J. P.; Barbieri, J.; Brown, E. B.; Gelbard, H. A. Mitochondrial Membrane Potential Probes and the Proton Gradient: A Practical Usage Guide. *BioTechniques* **2011**, *50*, 98−115.
(48) Eisner, D. A.; Nichols, C. G.; O'Neill, S. C.; Smith, G. L.; Valdeolmillos, M. The Effect of Metabolic Inhibition on Intracellular Calcium and pH in Isolated Rat Ventricular Cells. *J. Physiol.* **1989**, *411*, 393−418.
(49) Liberti, M. V.; et al. The Warburg Effect: How Does It Benefit Cancer Cells? *Trends Biochem. Sci.* **2016**, *41*, 211−218.
(50) Kondapalli, K. C.; Llongueras, J. P.; Capilla-González, V.; Prasad, H.; Hack, A.; Smith, C.; Guerrero-Cázares, H.; Quiñones-Hinojosa, A.; Rao, R. A Leak Pathway for Luminal Protons in Endosomes Drives Oncogenic Signalling in Glioblastoma. *Nat. Commun.* **2015**, *6*, No. 6289.
(51) Di Domenico, F.; Foppoli, C.; Blarzino, C.; Perluigi, M.; Paolini, F.; Morici, S.; Coccia, R.; Cini, C.; De Marco, F. Expression of Human Papilloma Virus Type 16 E5 Protein in Amelanotic Melanoma Cells Regulates Endo-Cellular pH and Restores Tyrosinase Activity. *J. Exp. Clin. Cancer Res.* **2009**, *28*, 4.
(52) Gohil, V. M.; Sheth, S. A.; Nilsson, R.; Wojtovich, A. P.; Lee, J. H.; Perocchi, F.; Chen, W.; Clish, C. B.; Ayata, C.; Brookes, P. S.; Mootha, V. K. Nutrient-Sensitized Screening for Drugs That Shift Energy Metabolism from Mitochondrial Respiration to Glycolysis. *Nat. Biotechnol.* **2010**, *28*, 249−255.
(53) Sabri, M. I.; Ochs, S. Inhibition of Glyceraldehyde-3-Phosphate Dehydrogenase in Mammalian Nerve by Iodoacetic Acid. *J. Neurochem.* **1971**, *18*, 1509−1514.
(54) Schmidt, M. M.; Dringen, R. Differential Effects of Iodoacetamide and Iodoacetate on Glycolysis and Glutathione Metabolism of Cultured Astrocytes. *Front. Neuroenerg.* **2009**, *1*, 1.
(55) Lutas, A.; Birnbaumer, L.; Yellen, G. Metabolism Regulates the Spontaneous Firing of Substantia Nigra Pars Reticulata Neurons via K ATP and Nonselective Cation Channels. *J. Neurosci.* **2014**, *34*, 16336−16347.
(56) Hung, Y. P.; Albeck, J. G.; Tantama, M.; Yellen, G. Imaging Cytosolic NADH-NAD(+) Redox State with a Genetically Encoded Fluorescent Biosensor. *Cell Metab.* **2011**, *14*, 545−554.
(57) Kauppinen, R. A.; Nicholls, D. G. Synaptosomal Bioenergetics: The Role of Glycolysis, Pyruvate Oxidation and Responses to Hypoglycaemia. *Eur. J. Biochem.* **1986**, *158*, 159−165.
(58) Tan, B.; Xiao, H.; Li, F.; Zeng, L.; Yin, Y. The Profiles of Mitochondrial Respiration and Glycolysis Using Extracellular Flux Analysis in Porcine Enterocyte IPEC-J2. *Anim. Nutr.* **2015**, *1*, 239−243.
(59) Duchen, M. R. Contributions of Mitochondria to Animal Physiology: From Homeostatic Sensor to Calcium Signalling and Cell Death. *J. Physiol.* **1999**, *516*, 1−17.
(60) Abad, M. F. C.; Di Benedetto, G.; Magalhães, P. J.; Filippin, L.; Pozzan, T. Mitochondrial pH Monitored by a New Engineered Green Fluorescent Protein Mutant. *J. Biol. Chem.* **2004**, *279*, 11521−11529.
(61) Casey, J. R.; Grinstein, S.; Orlowski, J. Sensors and Regulators of Intracellular pH. *Nat. Rev. Mol. Cell Biol.* **2010**, *11*, 50−61.
(62) Shen, Y.; Chen, Y.; Wu, J.; Shaner, N. C.; Campbell, R. E. Engineering of MCherry Variants with Long Stokes Shift, Red-Shifted Fluorescence, and Low Cytotoxicity. *PLoS One* **2017**, *12*, No. e0171257.
(63) Allen, M. D.; Zhang, J. Subcellular Dynamics of Protein Kinase A Activity Visualized by FRET-Based Reporters. *Biochem. Biophys. Res. Commun.* **2006**, *348*, 716−721.
(64) Komatsu, N.; Aoki, K.; Yamada, M.; Yukinaga, H.; Fujita, Y.; Kamioka, Y.; Matsuda, M. Development of an Optimized Backbone of FRET Biosensors for Kinases and GTPases. *Mol. Biol. Cell* **2011**, *22*, 4647−4656.
(65) Fritz, R. D.; Letzelter, M.; Reimann, A.; Martin, K.; Fusco, L.; Ritsma, L.; Ponsioen, B.; Fluri, E.; Schulte-Merker, S.; van Rheenen, J.; Pertz, O. A Versatile Toolkit to Produce Sensitive FRET Biosensors to Visualize Signaling in Time and Space. *Sci. Signal.* **2013**, *6*, rs12.
(66) Thestrup, T.; Litzlbauer, J.; Bartholomäus, I.; Mues, M.; Russo, L.; Dana, H.; Kovalchuk, Y.; Liang, Y.; Kalamakis, G.; Laukat, Y.; Becker, S.; Witte, G.; Geiger, A.; Allen, T.; Rome, L. C.; Chen, T.-W.; Kim, D. S.; Garaschuk, O.; Griesinger, C.; Griesbeck, O. Optimized Ratiometric Calcium Sensors for Functional in Vivo Imaging of Neurons and T Lymphocytes. *Nat. Methods* **2014**, *11*, 175−182.
(67) Filippin, L.; Abad, M. C.; Gastaldello, S.; Magalhães, P. J.; Sandonà, D.; Pozzan, T. Improved Strategies for the Delivery of GFP-Based Ca^{2+} Sensors into the Mitochondrial Matrix. *Cell Calcium* **2005**, *37*, 129−136.
(68) Xia, Z.; Dudek, H.; Miranti, C. K.; Greenberg, M. E. Calcium Influx via the NMDA Receptor Induces Immediate Early Gene Transcription by a MAP Kinase/ERK-Dependent Mechanism. *J. Neurosci.* **1996**, *16*, 5425−5436.

DOI: 10.1021/acsomega.8b00655
ACS Omega 2018, 3, 9476−9486